CALPHAD: Computer Coupling of Phase Diagrams and Thermochemistry 46 (2014) 108–117

Contents lists available at ScienceDirect

CALPHAD: Computer Coupling of Phase Diagrams and Thermochemistry

journal homepage: www.elsevier.com/locate/calphad

# Thermodynamic assessment of orientationally disordered organic molecular crystals: Ternary system pentaerythritol–neopentylglycol–2-amino-2methyl-1,3, propanediol (PE–NPG–AMPL)

Amrita Mishra, Anjali Talekar, Renhai Shi, Dhanesh Chandra *

*Chemical and Materials Engineering Department (MS388), University of Nevada, Reno, NV 89557, USA*

ARTICLE INFO

*Article history:*
Received 3 January 2013
Received in revised form
15 February 2014
Accepted 21 February 2014
Available online 15 March 2014

*Keywords:*
Ternary phase diagrams
Pentaerythritol
Neopentylglycol
2-Amino-2methyl-1,3,propanediol
Polyalcohols
Amines

ABSTRACT

Organic crystals such as pentaerythritol [PE-$C(CH_2OH)_4$], neopentylglycol [NPG-$(CH_3)_2C(CH_2OH)_2$] and 2-amino-2methyl-1,3,propanediol [AMPL-$(HOCH_2)_2C(NH_2)CH_3$] store a large amount of thermal energy in their solid state high temperature phases with orientational disorder. There are very few pure compounds of these polyalcohol and amine family that are commercially available exhibiting these properties, leading to limited choices of energy storage materials. Binary and ternary solid solutions allow a wider selection of materials with different phase transition temperature, heat content, and compositions for practical applications. Thermodynamic calculations of the PE–NPG–AMPL system are presented that provide critical thermodynamic data for energy storage systems. Substitutional solution model is used for optimization of interaction parameters. Activities of binaries, ternary isotherms of PE–NPG–AMPL at various temperatures, and pseudo-binary isopleth are presented.



## 1. Introduction

The driving force behind the development of renewable energy source is the emission of greenhouse gases and increasing fuel prices. Researchers are continually in search of new and alternative energy solutions, and solar radiation is considered to be one of the most promising sources of energy. One of the options is the development of energy storage devices, which are equally important as developing new energy sources. The development of thermal energy storage materials is important as a passive system in which energy stored during the day from solar radiation and utilized at later periods of time. Thermal energy can be stored as either sensible heat or as latent heat, in which heat is stored and released as these materials undergo phase transitions at nearly constant temperature. In general, "Phase Change Materials" (PCMs) can exhibit solid–liquid, liquid–gas or solid–solid phase transitions. Materials such as paraffins and salts store energy while undergoing solid–liquid phase transitions, but have a propensity to leak in containers, as well as exhibit super cooling effects [1]. In this study, we present a special class of energetic solid–solid phase change materials, with high entropy of solid–solid and low entropy of solid–liquid phase changes, referred to as "Orientationally Disordered Organic Molecular Crystals. These crystalline organic molecular materials are classified as "Plastic Crystals" in which portions of a molecules can rotate around one or several axes [2]. The formation of plastic crystals is attributed to the ability of the pseudospherical molecules to arrange themselves in a cubic array (FCC /BCC) over a particular range of temperature [3]. They also undergo thermal rotatory displacements at the same time, so that there is no long range orientational order between the molecules [4,5]. This phase is also referred to as ODIC (Orientational Disorder in Crystals) [6]. At the upper temperature limit of this orientational disordered phase the liquefaction occurs with breakdown of the long range positional order with only a small entropy variation, generally smaller than 21 $J\,mol^{-1}\,K^{-1}$ a characteristic value to classify these compounds and plastic crystal from a thermodynamic point of view [7]. Fig. 1 shows the structures of the compounds studied in this work. The advantage of these materials is that they utilize the heat capacity as well as the solid–solid latent heat of phase transitions. The focus of this research is the potential use of these materials in thermal energy storage and systems for solar and other applications, owing to the large entropy variation in the phase transitions.

Pentaerythritol and related organic crystals undergo solid–solid phase transformations, from low temperature $\alpha$ or $\beta$ layered or chained structures (tetragonal, monoclinic, orthorhombic) to isotropic disordered high temperature cubic ODIC (FCC or BCC) phases. Examples of these 'plastic crystals' include pentaerythritol [PE: C

* Corresponding author.
*E-mail addresses:* chandra12321@yahoo.com, dchandra@unr.edu (D. Chandra).

http://dx.doi.org/10.1016/j.calphad.2014.02.003
0364-5916/

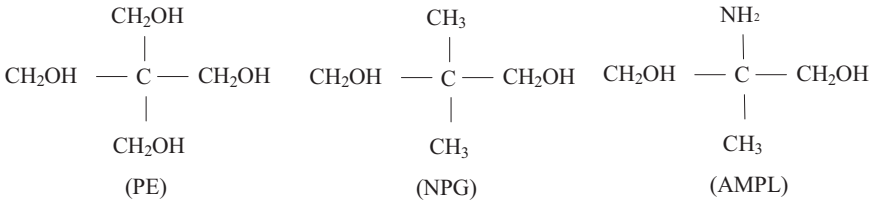


**Fig. 1.** Structure of PE, NPG and AMPL.

$(CH_2OH)_4$, 2-amino-2methyl-1,3, propanediol [AMPL: $(HOCH_2)_2C(NH_2)CH_3$], pentaglycerine [PG: $(CH_3)_2C(CH_2OH)_3$], neopentylglycol [NPG: $(CH_3)_2C(CH_2OH)_2$], and tris(hydroxymethyl)aminomethane [TRIS: $(NH_2)C(CH_2OH)_3$]. The thermodynamic parameters and crystallographic details for a number of such pure compounds and their binary system have been reported in the literature. Calculated phase diagrams for most of the systems have been reported by various investigators. To our knowledge, no ternary phase diagrams have been reported in these types of systems. This work aims at creating a calculated PE–NPG–AMPL ternary phase diagram. Nitta and Watanabe [8] reported crystallographic properties of the PE compound. Chandra et al. [9] used high resolution Guinier diffraction and reported high temperature structural details of PE and NPG. These polyalcohols when combined to form solid solutions undergo a variation in the phase transition temperatures. The solid solutions can then be used to suit particular applications [10]. To study the alloying effect on the solid–solid phase transitions, Benson et al. [11] investigated binary systems such as PE–PG, PE–NPG, and PG–NPG for thermal energy storage in solar buildings. Font et al. [12] carried out calorimetric studies of the mixtures of PE–NPG and PG–NPG and Barrio et al. [13] conducted an investigation of heat storage applicability of PE–PG, PG–NPG, and PE–NPG binary systems. Chandra et al. [14,15] reported a reduction in the transition temperature of PE by alloying it with PG and NPG. Several research groups have reported partial and complete phase diagrams of PG–NPG [16,17], PE–NPG [18–23], TRIS–NPG [24,25], PE–PG [26], TRIS–PG [27], TRIS–PE [28], TRIS–AMPL [29], and PE–AMPL [30]. Sturz et al.[31], Witusiewicz et al. [32], and Lopez et al. [33] reported thermodynamic assessment of similar systems that were carried out by other research groups to determine multicomponent phase equilibria.

Chandra et al. [34] determined the complete phase diagram for the AMPL–NPG binary. Barrio et al. [35] also reported on the AMPL–NPG binary, but there were significant differences between these two phase diagrams of Chandra et al. and Barrio et al. Salud et al. [36] performed further experimental studies on the AMPL–NPG system in 1997 including a calculated phase diagram. Chellappa et al. also published calculated phase diagrams for AMPL–NPG [37] and PE–AMPL [38]. AMPL–NPG phase diagrams have also been calculated by Witusiewicz et al. [32] using the CALPHAD method. A thermodynamic assessment of the ternary system PE–PG–NPG has been calculated using the CALPHAD method [39].

This work involves thermodynamic assessments of the PE–NPG, AMPL–NPG and PE–AMPL binary systems utilizing the CALPHAD method. In the case of NPG–AMPL system, we made two different calculations based on by Witusiewicz et al. [32], and Raja et al. [37]. These calculated binary phase diagrams are then used to compute the PE–NPG–AMPL ternary system.

## 2. Computational procedure

In order to compute phase equilibria and calculate the phase diagrams, certain thermodynamic parameters need to be calculated. This section describes the determination of thermodynamic properties (enthalpies and entropies of formation for PE, NPG and AMPL, Gibbs free energies of the stable and metastable phases, etc.).

### 2.1. Calculation of thermodynamic properties

Joback's group contribution method has been used to calculate the enthalpy and entropy of formation. Since, the organic plastic crystals (e.g. PE, NPG, AMPL) are not pure elements; their enthalpy of formation is not zero. These thermophysical quantities can be calculated using group contribution methods, which takes into account the smallest constituents (atoms/groups), and in this case, the functional groups (which may be composed of few atoms and bonds). Data for the functional groups is taken from Marrero and Gani [40]:

AMPL $(NH_2)(CH_3)C(CH_2OH)_2$

$$\Delta H_{AMPL} = \begin{pmatrix} -22.01 \\ -76.5 \\ 82.23 \\ -20.64 \\ -208.4 \end{pmatrix}, k = (1 \quad 1 \quad 1 \quad 1 \quad 2), \quad \Delta G_{AMPL} = \begin{pmatrix} 14.07 \\ -43.96 \\ 116.02 \\ 8.42 \\ -189.2 \end{pmatrix}$$

$$\Delta H_{0_{AMPL}} = (68.29 + k.\Delta H_{AMPL}) \times 10^3 = -406,030 \text{ kJ/mol}$$

$$\Delta G_{0_{AMPL}} = (53.88 + k.\Delta G_{AMPL}) \times 10^3 = -221,550 \text{ kJ/mol}$$

$$S_{0_{AMPL}} = \frac{\Delta H_{0_{AMPL}} - \Delta G_{0_{AMPL}}}{298} = -619.06 \text{ kJ/mol K}$$

**NPG** $(CH_3)_2C(CH_2OH)_2$

$$\Delta H_{NPG} = \begin{pmatrix} -76.45 \\ 82.2 \\ -20.64 \\ -208.04 \end{pmatrix}, k = (2\ 1\ 2\ 2)$$

$$\Delta H_{0_{NPG}} = (68.29 + k.\Delta H_{NPG}) \times 10^3 = -459,770 \text{ kJ/mol}$$

$$\Delta G_{0_{NPG}} = (53.88 + k.\Delta G_{NPG}) \times 10^3 = -279,580 \text{ kJ/mol}$$

$$S_{0_{AMPL}} = \frac{\Delta H_{0_{NPG}} - \Delta G_{0_{NPG}}}{298} = -604.66 \text{ kJ/mol K}$$

### 2.2. Thermodynamic modeling of solution phases

The low temperature phases of pure compounds are referred to as "Phase III" or "Phase II,' and the high temperature phases as "Phase I." The nomenclature used for low temperature phases is $\alpha$, $\beta$ or $\delta$ phases, and for high temperature phases as $\gamma$, $\varepsilon$ or $\eta$, in the multicomponent system. For simplicity PE is represented by "A," NPG as "B" and AMPL as "C." Table 1 shows list of symbols used to describe the various phases in the PE–NPG–AMPL ternary system.

A CALPHAD type optimization using regular and sub-regular solution model is considered to be adequate to describe the Gibbs energies of different phases. If the reference state for each phase is taken to be that of the pure components in that phase, then the Gibbs energy of a solution phase $\phi$ ($\phi = \alpha, \beta, \delta, \gamma, \varepsilon, \theta, \eta, L$) can be represented as follows (unit of Gibbs energy is J $mol^{-1}$ throughout

**Table 1**
List of symbols denoting phases in PE–NPG–AMPL system.

| Symbol | Phase |
|---|---|
| Liq or $L$ | Liquid |
| $\alpha$ | Low temperature PE phase |
| $\beta$ | Low temperature NPG phase |
| $\delta$ | Low temperature AMPL phase |
| $\gamma$ | High temperature PE phase |
| $\varepsilon$ | High temperature NPG phase |
| $\eta$ | High temperature AMPL phase |

this work, where a mol is a mole of formula unit):

$$G^{\phi} = x_A {}^0G_A^{\phi} + x_B {}^0G_B^{\phi} + + x_C {}^0G_C^{\phi} + RT(\ln x_A + \ln x_B + \ln x_C) + G^{EX,\phi}$$

where $\phi = \alpha, \beta, \delta, \gamma, \varepsilon, \theta, \eta, L$, $R = 8.314\ \mathrm{J\ mol^{-1}\ K^{-1}}$, $x_A$ is the mole fraction of "A", $x_B$ is the mole fraction of "B" and $x_C$ is the mole fraction of "C". ${}^0G_A^{\phi}$, ${}^0G_B^{\phi}$ and ${}^0G_C^{\phi}$ are the pure component Gibbs energies in $\phi$.

The excess Gibbs energy for a binary system A–B, can be demoted as

$$G_{mix}^{EX} = x_A x_B (L_{AB}^0 + L_{AB}^1 (x_A - x_B))$$

The binary interaction parameters for excess Gibbs energies, $L_{i,j}^{\phi}$ can be expressed as follows:

$$L_{i,j}^{\phi} = \sum_{n=0}^{m} {}^nL_{i,j}^{\phi} (x_i - x_j)$$

The ternary excess Gibbs free energy is written as follows:

$$G_{mix}^{EX} = x_A x_B (L_{AB}^0 + L_{AB}^1 (x_A - x_B)) + x_B x_C (L_{BC}^0 + L_{BC}^1 (x_B - x_C)) + x_A x_C (L_{AC}^0 + L_{AC}^1 (x_A - x_C))$$

The binary and the ternary interaction parameters ${}^nL_{i,j}^{\phi}$ and ${}^nL_{i,j,k}^{\phi}$ take the following form:

$${}^nL_m^{\phi} = a + bT + cT\ln(T) + dT^2 + eT^{-1} + fT^3 + gT^7 + hT^{-9}$$

where $a,b,c,d,e,f,g$ and $h$ are the excess Gibbs energy parameters. In most cases only the first two terms of the above equation are used.

For a phase $\phi$ ($\phi = \alpha, \beta, \delta, \gamma, \varepsilon, \eta, L$), ${}^0G_A^{\phi}$, ${}^0G_B^{\phi}$ and ${}^0G_C^{\phi}$ are the reference states of pure "A", "B" and "C", same as $\phi$. A single reference phase is chosen for each component.

The reference phases were chosen and denoted as: $\alpha$ for "A", $\beta$ for "B" and $\delta$ for "C" and set to zero.

Therefore,

$${}^0G_A^{\alpha} = 0, \quad {}^0G_B^{\beta} = 0 \text{ and } {}^0G_C^{\delta} = 0$$

The binary phase diagrams are calculated first and extrapolated to a ternary system. The stable phases for "A" are $\alpha$, and $\gamma$, $\varepsilon$ and $\beta$ for "B" and $\theta$ and $\delta$ for "C". Gibbs energies of the other phases in terms of these reference states can be represented as follows:

For system A–B (PE–NPG), the Gibbs energies of the other phases in terms of the reference phases can be represented as

$${}^0G_A^{\gamma} = {}^0G_A^{\alpha} + \Delta^0G_A^{\alpha\to\gamma} = \Delta^0G_A^{\alpha\to\gamma}$$
$${}^0G_A^{L} = {}^0G_A^{\alpha} + \Delta^0G_A^{\alpha\to L} = \Delta^0G_A^{\alpha\to\gamma} + \Delta^0G_A^{\alpha\to L}$$
$${}^0G_B^{\varepsilon} = {}^0G_B^{\beta} + \Delta^0G_B^{\beta\to\varepsilon} = \Delta^0G_B^{\beta\to\varepsilon}$$
$${}^0G_B^{L} = {}^0G_B^{\beta} + \Delta^0G_B^{\beta\to L} = \Delta^0G_A^{\beta\to\varepsilon} + \Delta^0G_B^{\beta\to L}$$

The pure Gibbs energies were determined using the heat capacity data. So, for component "A" the Gibbs energies of the stable phases are

$${}^0G_A^{\gamma} = {}^0G_A^{\alpha} + \Delta^0G_A^{\alpha\to\gamma} = \Delta^0G_A^{\alpha\to\gamma}$$

$${}^0G_A^{\gamma} = \Delta H_{TR} - T\Delta S_{TR} + \int_{T_{TR}}^{T} \Delta C_P^{\alpha\to\gamma} dT - T\int_{T_{TR}}^{T} \frac{\Delta C_P^{\alpha\to\gamma}}{T} dT$$

Similar expressions can be obtained for Gibbs energies of stable phases of "B" and "C".

### 2.3. Metastable phase calculations

The Gibbs energies for metastable phases are estimated by modifications to the stable phases. For example, for " A" in $\beta$ phase, we are interested in determining the difference, ${}^0G_A^{\beta} - {}^0G_A^{\alpha}$, such that we can express

$${}^0G_A^{\beta} = {}^0G_A^{\alpha} + M_A^{\beta}$$

The Gibbs energy of the $\beta$ phase, $G_m^{\beta}$, can now be written as

$$G_m^{\beta} = x_A({}^0G_A^{\alpha} + M_A^{\beta}) + x_B {}^0G_B^{\beta} + RT \times (x_A \ln x_A + x_B \ln x_B) + G^{EX,\beta}$$
$$G_m^{\beta} = x_A M_A^{\beta} + RT \times (x_A \ln x_A + x_B \ln x_B) + G^{EX,\beta}$$

Similarly for the $\alpha$ phase, we can write the Gibbs free energy, $G_m^{\alpha}$, as

$$G_m^{\alpha} = x_A {}^0G_A^{\alpha} + x_B({}^0G_B^{\beta} + M_B^{\alpha}) + RT \times (x_A \ln x_A + x_B \ln x_B) + G^{EX,\alpha}$$
$$G_m^{\beta} = x_B M_B^{\alpha} + RT \times (x_A \ln x_A + x_B \ln x_B) + G^{EX,\alpha}$$

To estimate $M_A^{\beta}$ and $M_B^{\alpha}$, $\alpha$ and $\beta$ phases are assumed to be ideal solutions. It should be noted that this assumption is based only for the purpose of calculating the metastable phases.

Therefore, the partial molar Gibbs free energies can be written as

$$G_B^{\beta} = {}^0G_B^{\beta} + RT\ln(x_B^{\beta})$$
$$G_B^{\alpha} = {}^0G_B^{\alpha} + RT\ln(x_B^{\alpha})$$

where, $G_B^{\beta}$ and $G_B^{\alpha}$ are the Gibbs energies of "B" in the $\beta$ and $\alpha$ phases respectively. At equilibrium, $G_B^{\beta} = G_B^{\alpha}$, the following estimation can be made at the temperature of maximum solubility (determined from experimental data), $T = T_{\max}$,

$${}^0G_B^{\alpha} = {}^0G_B^{\beta} + RT_{\max} \ln\left(\frac{x_{B(\max)}^{\beta}}{x_{B(\max)}^{\alpha}}\right)$$

$${}^0G_B^{\alpha} = RT_{\max} \ln\left(\frac{x_{B(\max)}^{\beta}}{x_{B(\max)}^{\alpha}}\right)$$

$$M_B^{\alpha} = RT_{\max} \ln\left(\frac{x_{B(\max)}^{\beta}}{x_{B(\max)}^{\alpha}}\right)$$
$$= 8.314 \times 283.15 \times \ln\left(\frac{0.96}{0.03}\right)$$
$$= 8158.7\ \mathrm{J\ mol^{-1}}$$

A similar estimation can be made for $M_A^{\beta}$ and is given by

$$M_A^{\beta} = RT_{\max} \ln\left(\frac{x_{A(\max)}^{\alpha}}{x_{A(\max)}^{\beta}}\right)$$
$$= 8.314 \times 283.15 \times \ln\left(\frac{0.97}{0.04}\right)$$

The assumption that $\alpha$ and $\beta$ phases are ideal solutions is used only to describe the metastable pure Gibbs energies ${}^0G_B^{\alpha}$ and ${}^0G_A^{\beta}$. The nature of non-ideality of $\alpha$ phase can still be expressed using a sub-regular solution model for $G^{EX,\alpha}$.

To estimate the metastable ${}^0G_A^{\varepsilon}$ and ${}^0G_B^{\gamma}$, we again assume ideal solutions and thus we can make the following estimations:

$${}^0G_A^{\varepsilon} = {}^0G_A^{\gamma} + RT_{\max} \ln\left(\frac{x_{A(\max)}^{\gamma}}{x_{A(\max)}^{\varepsilon}}\right)$$

$$= \Delta^0 G_A^{\alpha\to\gamma} + RT_{\max} \ln\left(\frac{x^{\gamma}_{A(\max)}}{x^{\varepsilon}_{A(\max)}}\right)$$

$$M_A^{\gamma} = RT_{\max} \ln\left(\frac{x^{\gamma}_{A(\max)}}{x^{\varepsilon}_{A(\max)}}\right)$$

$$= 8.314 \times 325.15 \times \ln\left(\frac{0.57}{0.48}\right)$$

$$= 404.5 \text{ J mol}^{-1}$$

Similarly,

$$M_B^{\varepsilon} = RT_{\max} \ln\left(\frac{x^{\varepsilon}_{B(\max)}}{x^{\gamma}_{B(\max)}}\right)$$

$$= 8.314 \times 325.15 \times \ln\left(\frac{0.51}{0.43}\right) = 461.25 \text{ J mol}^{-1}$$

## 3. Experimental data

### 3.1. Phase equilibria

Most of the descriptions of the enthalpies and transition temperatures were obtained from Murrill and Breed [10] and are shown in Table 1. The enthalpies and the phase transition temperatures for AMPL were taken from Murrill and Breed [10]. Data for pure AMPL reported by Chandra et al. [34] is higher than the data available in literature. The transition temperatures of the compounds used by Salud et al. [36] were higher than that used in earlier works [41,42]. The reason for the difference in the data can be attributed to this fact. These data have been used for the thermodynamic calculations in this work. Enthalpies and phase transition temperatures for pure PE and NPG used for calculations were taken from Eilerman et al. [43]. The data that is available for these kinds of organic systems are essentially the tie lines and invariant equilibria determined by using DSC and X-ray diffraction.

### 3.2. AMPL–NPG binary phase diagram

The AMPL–NPG binary phase diagram has been previously calculated using the CALPHAD method by Witusiewicz et al. [32] and Chellappa and Chandra [37]. Witusiewicz et al. [32] reported that the data from Chandra et al. [34] gave a lower eutectic temperature. They attributed the difference to a lower purity of AMPL (99%) used. Binary phase diagram of AMPL–NPG has also been calculated using data from Witusiewicz et al. [32] for comparison.

### 3.3. PE–AMPL binary phase diagram

The PE–AMPL system has been calculated previously by Chellappa et al. [38] using the CALPHAD method. Chellappa et al. [38] used pure PE data from Chandra et al. [44] and pure AMPL data from Barrio et al. [45] as well as Murrill and Breed [10]. The calculated slopes for the liquidus and solidus boundaries for the two-phase $\gamma+L$ and $\eta+L$ systems were tested for thermodynamic consistency using the equation given in Pelton [46]. Pelton [46] provides an method for checking the thermodynamic consistency of the slopes of phase boundaries in the liquidus region by determining the enthalpies of fusion from the slopes as follows:

$$(dT/dX_A^L)^{-1}_{x_A=1} - (dT/dX_A^S)^{-1}_{x_A=1} = \Delta H^0_{F(A)}/R(T^0_{F(A)})^2$$

### 3.4. PE–NPG binary phase diagram

The PE–NPG binary phase diagram is reported by different groups with significant differences in their observations [47,48,49]. Barrio et al. [47] reported the existence of an intermediate cubic phase. They reported an invariant temperature as 70.6 °C (343.6 K), produced by the presence of a new phase. Teisseire et al. [49] also developed the PE–NPG binary phase diagram using calorimetry and X-ray diffraction but they did not notice the presence of an intermediate cubic phase as reported by Barrio et al. [47]. Tesseire et al. [49] noted a solid–liquid phase at 165 °C (438 K) in the PE–NPG system, whereas Chandra et al. [50] showed a two phase region consisting of two individual high temperature phase regions. Barrio et al. [47] proposed a PE–NPG phase in the temperature range from room temperature to 393 K. They observed invariant equilibria at 343.6 K which does not correspond to the phase diagrams proposed by Tesseire et al. [49] and Chandra et al. [50]. The PE–NPG phase diagram by Chandra et al. [51] was calculated using the FACT Sage program. There is a good agreement between the phase diagrams calculated by Chandra et al. [48] and proposed by Tesseire et al. [49]. The major difference between the two above mentioned phase diagrams are that Tesseire et al. [49] predicted a two phase (solid–liquid) region at about 163 °C (436 K), whereas Chandra et al. [51] predicted the presence of a two phase region consisting of two high temperature solid phases belonging to PE and NPG each at the same temperature. Barrio et al. pointed out that since the two

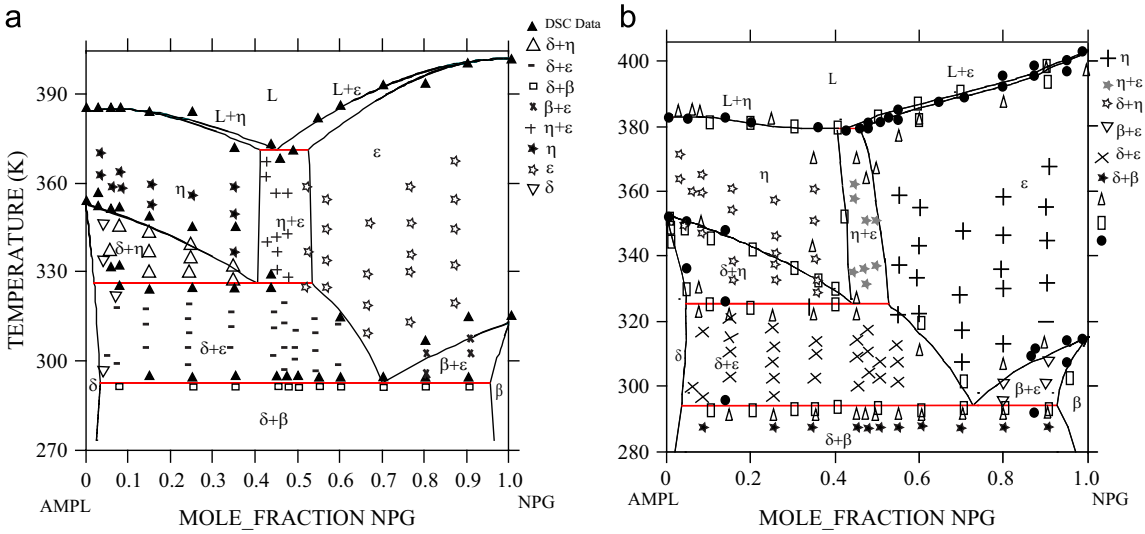


**Fig. 2.** AMPL–NPG phase diagram (a) Chellappa and Chandra [37] and (b) Witusiewicz et al. [32].

**Table 2**

(a) Expressions for Gibbs energies of pure components (NPG–AMPL) (Chellappa and Chandra [37]).

| No. | Gibbs energy expression |
|---|---|
| NPG–AMPL | |
| 1 | ${}^0G^{\beta}_{NPG} = 0$ |
| 2 | ${}^0G^{\delta}_{AMPL} = 0$ |
| 3 | ${}^0G^{\delta}_{NPG} = 8158.7$ |
| 4 | ${}^0G^{\beta}_{AMPL} = 7505.88$ |
| 5 | ${}^0G^{\varepsilon}_{NPG} = 13,630 - 43.55T + 0.351T^2 + 1621.98T - 51,061.57 - 272.99T\ln(T)$ |
| 6 | ${}^0G^{\eta}_{AMPL} = 23,300 - 66.01T - 0.275T^2 + 949.46T - 73,097.48 - 110T\ln(T)$ |
| 7 | ${}^0G^{\eta}_{NPG} = 13,630 - 43.55T + 0.351T^2 + 1621.98T - 51,061.57 - 272.99T\ln(T) + 461.25$ |
| 8 | ${}^0G^{\varepsilon}_{AMPL} = 23,300 - 66.01T - 0.275T^2 + 949.46T - 73,097.48 - 110T\ln(T) + 404.55$ |
| 9 | ${}^0G^{L}_{NPG} = 18,315 - 55.2T + 0.425T^2 + 2098.38T - 69,849.68 - 349.613T\ln(T)$ |
| 10 | ${}^0G^{L}_{AMPL} = 26,291.4 - 73.77T - 0.29T^2 + 1026.62T - 78,953.7 - 119.44T\ln(T)$ |

(b) Summary of the thermodynamic parameters of the solution phases in the AMPD–NPG system (in J $mol^{-1}$) (Witusiewicz et al. [32])

| Phase | Parameters |
|---|---|
| Liquid | ${}^0L^{LIQ}_{AMPD,NPG} = -11,119.7 + 32.1547T$, ${}^1L^{LIQ}_{AMPD,NPG} = -675.7$ |
| BCC_A2 | ${}^0G^{BCC\_A2}_{NPG} = 550 + {}^0G^{FCC\_A1}_{NPG}$, ${}^0L^{BCC\_A2}_{AMPD,NPG} = -10,369.8 + 29.0726T$, ${}^1L^{BCC\_A2}_{AMPD,NPG} = -506.5$ |
| FCC_A1 | ${}^0G^{FCC\_A1}_{AMPD} = 510 + {}^0G^{BCC\_A2}_{AMPD}$, ${}^0L^{FCC\_A1}_{AMPD,NPG} = -9577.8 + 26.7008T$, ${}^1L^{FCC\_A1}_{AMPD,NPG} = 4505.4 - 15.0091T$ |
| Monoclinic | ${}^0L^{MONOCL}_{AMPD,NPG} = 34,834.5 - 91.6551T$, ${}^1L^{MONOCL}_{AMPD,NPG} = 85,12.9 + 31.3862T$ |
| AMPD-II | ${}^0G^{AMPD-II}_{NPG} - H^{SER}_{NPG} = 5500 + GH^{SER}_{NPG}$ |
| NPG-II | ${}^0G^{NPG-II}_{AMPD} - H^{SER}_{AMPD} = 8000 + GH^{SER}_{AMPD}$ |

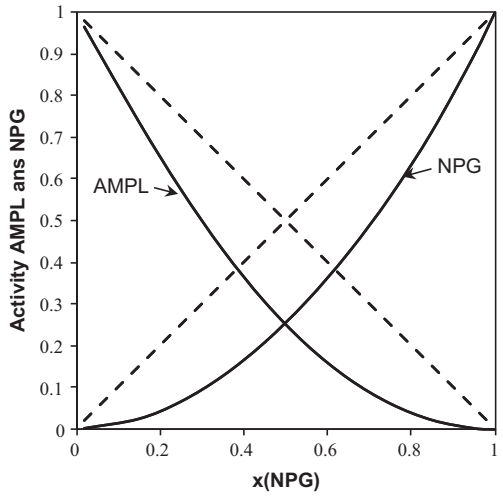


**Fig. 3.** Activity of AMPL–NPG at 340 K.

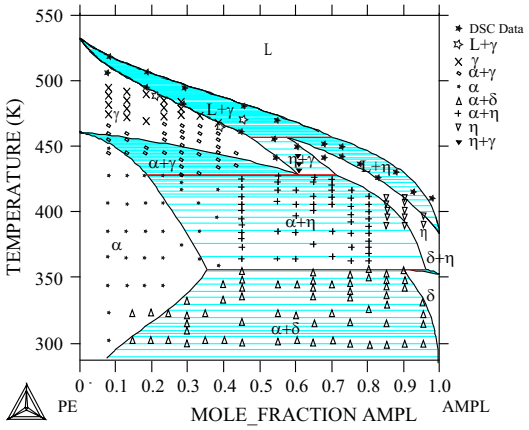


**Fig. 4.** PE–AMPL phase diagram (modeled using data from Chellappa et al. [38]).

substances are isomorphic at high temperatures a new phase might appear [47].

## 4. Results and discussion

### 4.1. Thermodynamic analysis

The binary systems were calculated first using ideal solution assumption with the inclusion of heat capacity. However, these results proved not to be satisfactory in the analysis. Therefore, the excess parameters were calculated using experimental data. To determine the excess Gibbs energy parameters, a thermodynamic optimization utilizing all available experimental data is desired [52]. The optimization to determine the excess Gibbs energy parameters was carried out using the PARROT module of the Thermo-Calc software [52,53]. Henrian, regular and sub-regular solution models were used to evaluate the excess parameters for the various phases. The details are summarized in this section.

### 4.2. AMPL–NPG binary system

The AMPL–NPG phase diagram was modeled using thermodynamic parameters of the solution phases from the work of Witusiewicz et al. [32] and Chellappa and Chandra [37] separately. The binary phase diagrams are presented in Fig. 2. For the ternary phase diagram, AMPL–NPG data from Witusiewicz et al. [32] was used (Gibbs energy equations and interaction parameters) as it is the most recent data available; however, we also show calculated phase diagram reported by Chellappa and Chandra [37] for comparison. The thermodynamic data of NPG–AMPL for Raja et al. [37] is shown Table 2(a), and the data for Witusiewicz et al. [32] is shown in Table 2(b). The activity of the AMPL–NPG mixture has been calculated from the excess Gibbs energy parameters and the activity plot at 340 K is shown in Fig. 3. The binary

**Table 3**
Expressions for Gibbs energies of pure components (PE–AMPL).

| No. | Gibbs energy expression |
|---|---|
| 1 | ${}^0G^{\alpha}_{PE}=0$ |
| 2 | ${}^0G^{\delta}_{AMPL}=0$ |
| 3 | ${}^0G^{\alpha}_{AMPL}=4381$ |
| 4 | ${}^0G^{\delta}_{PE}=7795$ |
| 5 | ${}^0G^{\gamma}_{PE}=41,260-89.5T+1.089T^2+6794.78T-272,492.72-1093.35T\ln(T)$ |
| 6 | ${}^0G^{\eta}_{AMPL}=23,300-66.01T-0.275T^2+949.46T-73,097.48-110T\ln(T)$ |
| 7 | ${}^0G^{\theta}_{PE_{AMPL}}=41,260-89.5T+1.089T^2+6794.78T-272,492.7-1093.35T\ln(T)+439$ |
| 8 | ${}^0G^{\gamma}_{AMPL}=23,300-66.01T-0.275T^2+949.46T-73,097.48-110T\ln(T)+324.2$ |
| 9 | ${}^0G^{L}_{PE}=46,280-98.92T+1.3765T^2+7119.4T-237,151.62-1180.015T\ln(T)$ |
| 10 | ${}^0G^{L}_{AMPL}=26,291.4-73.33T-0.29T^2+1026.62T-78,953.7-119.44T\ln(T)$ |

**Table 4**
Expressions for Gibbs energies of pure components (PE–NPG).

| No. | Gibbs energy expression |
|---|---|
| PE–NPG | |
| 1 | ${}^0G^{\alpha}_{PE}=0$ |
| 2 | ${}^0G^{\beta}_{NPG}=0$ |
| 3 | ${}^0G^{\beta}_{PE}=25,000-10T$ |
| 4 | ${}^0G^{\alpha}_{NPG}=20,000-40T$ |
| 5 | ${}^0G^{\gamma}_{PE}=41,260-89.5T+1.089T^2+6794.7T-272,492.7-1093.35T\ln(T)$ |
| 6 | ${}^0G^{\varepsilon}_{NPG}=13,630-43.54T+0.35T^2+1621.98T-51,061.5-272.9T\ln(T)+1028$ |
| 7 | ${}^0G^{\varepsilon}_{PE}=41,260-89.5T+1.089T^2+6794.7T-272,492.7-1093.35T\ln(T)+1341$ |
| 8 | ${}^0G^{\varepsilon}_{NPG}=13,630-43.54T+0.35T^2+1621.98T-51,061.5-272.9T\ln(T)$ |
| 9 | ${}^0G^{L}_{NPG}=18,315-55.2T+0.425T^2+2098.38T-69,849.69-349.613T\ln(T)$ |
| 10 | ${}^0G^{L}_{PE}=46,280.-98.92T+1.3765T^2+7119.64T-237,151.63-118.015T\ln(T)$ |

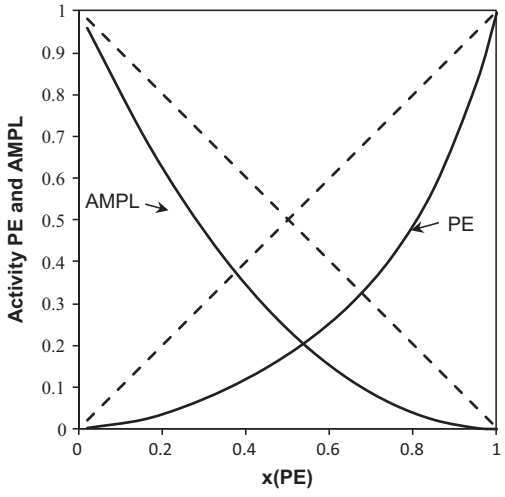


**Fig. 5.** Activity of PE–AMPL at 340 K.

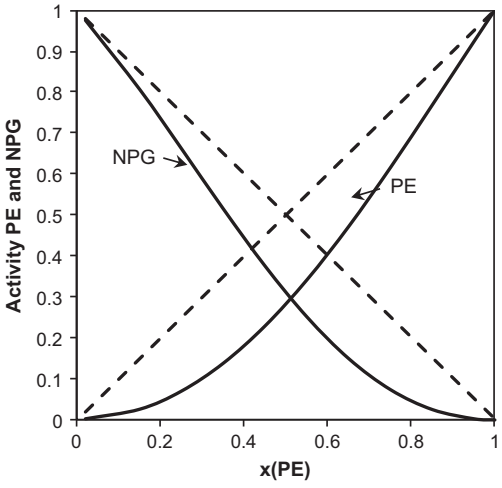


**Fig. 7.** Activity of PE–NPG at 340 K.

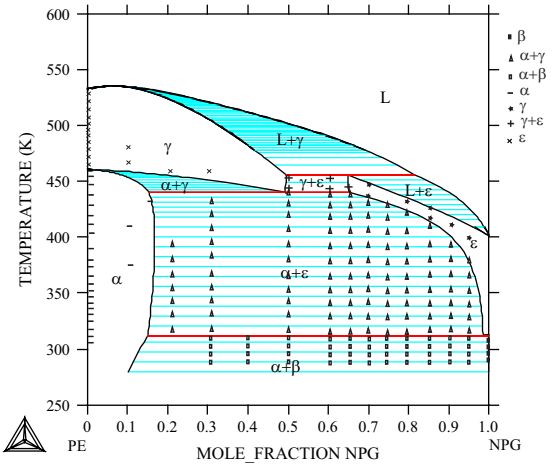


**Fig. 6.** PE–NPG phase diagram. Data points from Chandra and Barrett [14].

phase diagrams in this work were used for calculations of PE–NPG–AMPL ternary diagrams.

The AMPL–NPG phase diagram reported earlier [37], agrees mostly with the experimental phase diagram, but invariant equilibria temperatures differed by 3–7 K. Salud et al. re-determined the AMPL–NPG system because of incoherencies in earlier reported works [36]. Chellappa and Chandra [37] compared the differences between excess parameters of their work with those of Salud et al. [36]. The low temperature phases are assumed as ideal phases in this work. This assumption was made because of limited miscibility of the low temperature phases. Witusiewicz et al. [32] calculated the AMPL–NPG (they denoted AMPL as AMPD) after Chellappa and Chandra [37] and saw discrepancies in the phase diagram; they noticed a difference of about 12–14 K in the eutectic temperature, although they did use data from Chandra et al. [34] for low temperature equilibria. The excess Gibbs free energies reported by Chellappa and Chandra [37] are

$$G^{EX,\delta}=x_Ax_B(676.9-3.11*T)$$
$$G^{EX,b}=x_Ax_B(42.48-1.96*T)$$
$$G^{EX,L}=x_Ax_B((242.4+1.93*T+175.19(x_A-x_B))$$
$$G^{EX,\varepsilon}=x_Ax_B((-202.2+2.19*T)+214.6(x_A-x_B))$$
$$G^{EX,\eta}=x_Ax_B((-394.2+2.72*T)+162.88(x_A-x_B)).$$

### 4.3. PE–AMPL binary system

The optimization of the PE–AMPL binary phase diagram was carried out using sub-regular solution models for the high temperature phases ($\gamma$ and $\eta$). Regular solution model was assumed for the low temperature phases ($\alpha$ and $\delta$), and the liquid solution was assumed to be ideal. In fact, most phase diagram calculations for these binary organic systems utilize temperature dependent sub-regular solution for high temperature phases [41,42]. The optimized phase diagram is presented in Fig. 4.

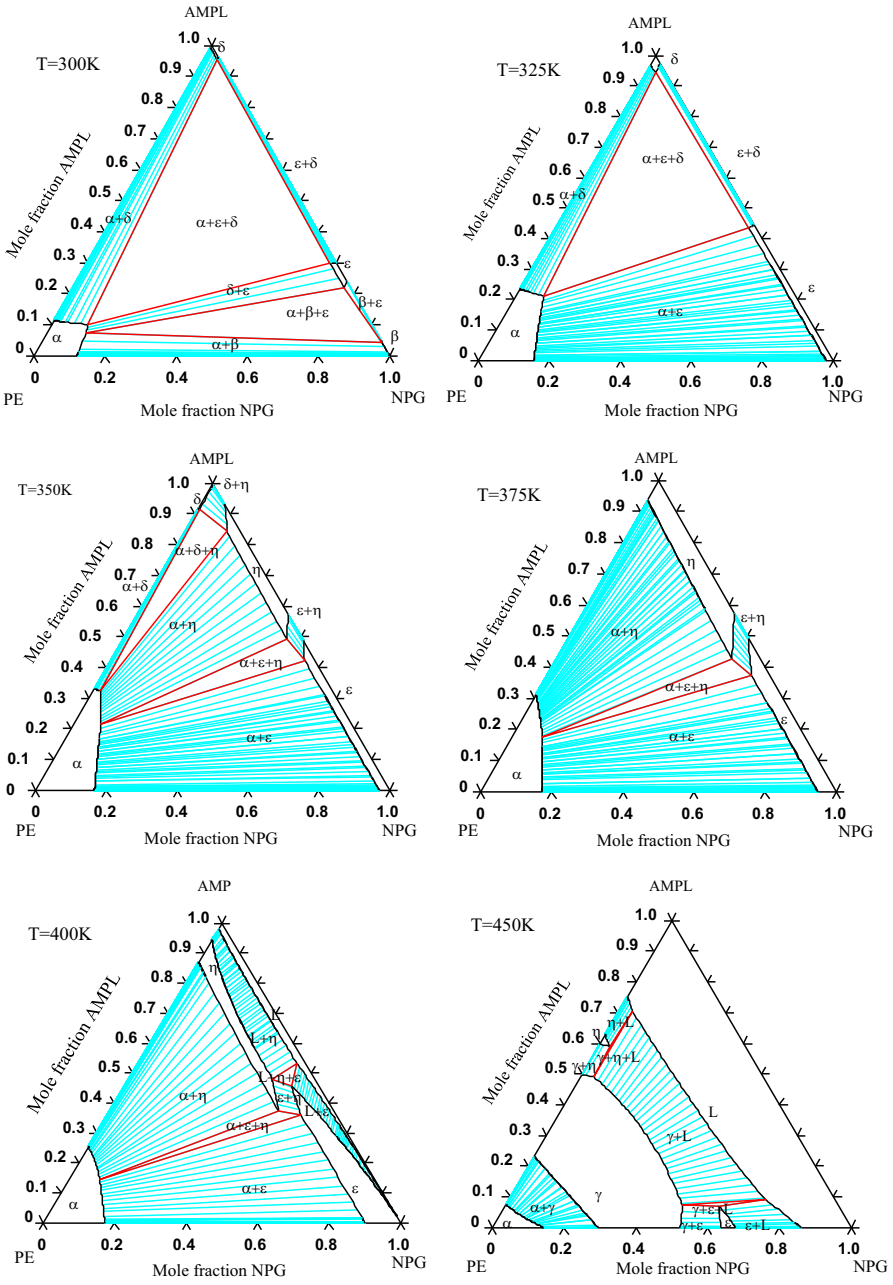


**Fig. 8.** Isotherms of PE–NPG–AMPL at various temperatures.

The ideal solution assumption is used for estimation of the Gibbs energies of the metastable phases. The following are the final optimized parameters for the PE–AMPL binary system:

$$G^{EX,\alpha} = x_A x_B(28413.46 - 90.32{*}T)$$
$$G^{EX,\delta} = x_A x_B(43320.87 - 130.69{*}T)$$
$$G^{EX,\gamma} = x_A x_B((-13041.06 + 28.26{*}T) + 2030.44\ (x_A - x_B))$$
$$G^{EX,\eta} = x_A x_B((840.95 - 2.44{*}T) + 449.42\ (x_A - x_B))$$
$$G^{EX,L} = x_A x_B(-712.05 + 453.9(x_A - x_B))$$

The interaction parameters were very close to the ones reported by Chellappa et al. for the calculation of the PE–AMPL system using the CALPHAD method and Thermo-Calc software [38].

The low temperature peritectoid was not shown by Russell [30]. Chellappa et al. [38] attributed this to the use of incorrect pure AMPL transition temperature (357 K) by Ding [44]. The use of the correct transition temperature (353 K) provided by Sigma-Aldrich company, shows the existence of a peritectoid. The calculated PE–AMPL phase diagram agrees with that calculated by Chellappa et al. [38] using CALPHAD method, that the two phase region $\delta+\eta$ (in this case), cannot exist above the invariant temperature. Table B.1 in Appendix shows the experimental invariant equilibria for the PE–AMPL system.

This two phase region has to be below the invariant temperature, in order to agree with Gibbs phase rule. Table 3 shows the Gibbs energy equations used for the calculation of PE–AMPL binary phase diagram. Pelton [46] explained the influence of regular solution parameters on phase boundaries. Using positive regular parameters for $\gamma$ and $\eta$, the liquid phase did 'not penetrate' into the low temperature $\alpha$ phase. Pelton [54] described the need for sub-regular parameters when the behavior of system is not symmetric with respect to concentration. This is indeed the case

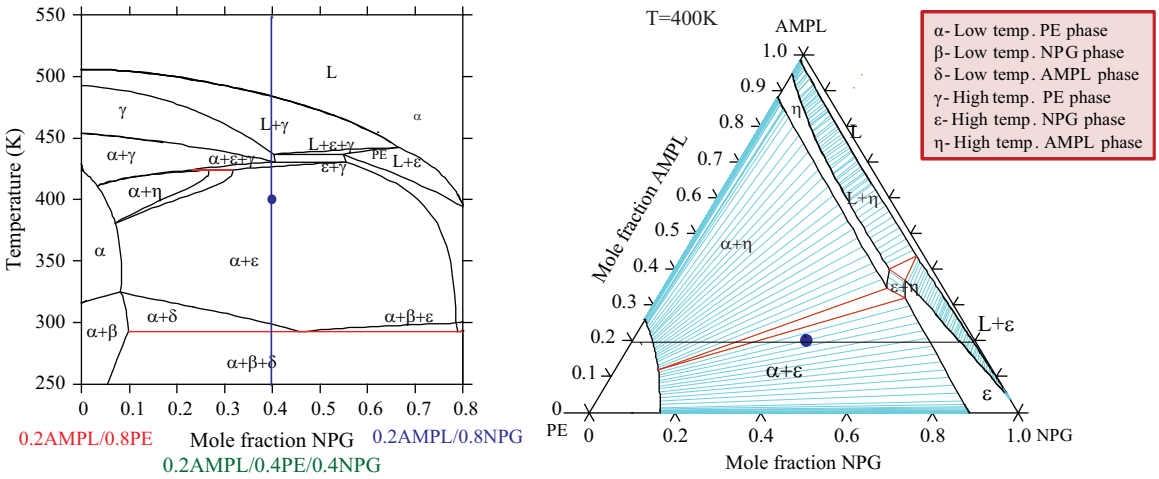


**Fig. 9.** Isopleth at 0.2AMPL/0.4PE/0.4NPG and ternary PE–NPG–AMPL. Please note that the dot in the pseudo-binary represents stable phases in the ternary diagram.

with PE–AMPL which does not exhibit symmetrical behavior like AMPL–NPG. Therefore, it was decided to use to sub-regular parameters for the high temperature $\gamma$ and $\eta$ phases. The calculated activities for the PE–AMPL system are shown in Fig. 5.

### 4.4. PE–NPG binary system

The PE–NPG system was optimized using Henrian solution model with temperature dependence. The optimized parameters for the binary system are given below:

$$G^{EX,\alpha} = x_A x_B(-2428.1-3.64*T)$$
$$G^{EX,\beta} = x_A x_B(2.1+1.69*T)$$
$$G^{EX,\varepsilon} = x_A x_B(939.8)$$
$$G^{EX,\gamma} = x_A x_B(877.34)$$
$$G^{EX,L} = x_A x_B(3116.5)$$

The calculated PE–NPG system is shown in Fig. 6. Tesseire et al. [49] noticed a solid–liquid phase at 165 °C (438 K), whereas Chandra et al. [50] noticed a two phase region consisting of two individual high temperature phase regions. Barrio et al. [47] proposed a PE–NPG phase in the temperature range from room temperature to 393 K. They observed invariant equilibria at 343.6 K which does not correspond to the phase diagrams proposed by Tesseire et al. and Chandra et al. [44,50]. The PE–NPG phase diagram by Chandra et al. was calculated using the FACT Sage program. There is good agreement between the phase diagrams calculated by Chandra et al. [44] and proposed by Tesseire et al.[49]. The major difference between the two above mentioned phase diagrams are that Tesseire et al. [49] predicted a two phase (solid–liquid) region ~163 °C, whereas Chandra et al. [44,50] predicted the presence of a two phase region consisting of two high temperature solid phases belonging to PE and NPG each at the same temperature. Barrio et al. [47] pointed out that since the two substances are isomorphic at high temperatures a new phase might appear. The reason that PE and NPG do not form a completely miscible solid solution in the high temperature region has been discussed in previous work [39]. When PE and NPG molecules bond in the high temperature phases, there is an increase in the $-CH_3$ dangling bonds, and the differences in the in the vibrational motions of the PE and NPG solid solution phases [26] results in limited miscibility and the formation of a two, $\gamma+\varepsilon$, phase region is observed. There is also a strong possibility of a metastable phase crossing the two-phase equilibria, as existence of the intermediate phase cannot be described without the introduction of a new metastable phase. Table 4 shows the Gibbs energy expressions for PE–NPG system. Fig. 7 shows the activity plot for PE and NPG, calculated from the interaction parameters.

### 4.5. Ternary PE–NPG–AMPL

The binary phase diagrams referenced above for the three systems have been used for a straight forward assessment of the metastable Gibbs energies along with optimization and estimation of interaction parameters. The binary phase diagrams are then used to calculate the ternary system (PE–NPG–AMPL). The following assumptions were made in order to estimate the number of phases present in the system:

Low temperature PE has tetragonal crystal structure, NPG has monoclinic and AMPL also has monoclinic structure for the low temperature phases. In spite of AMPL and NPG being monoclinic, there is very limited solubility between the two compounds as can be seen from the AMPL–NPG phase diagram. So, it is a reasonable assumption that that the low temperature for the ternary phases consist of three phases (which are predominantly PE, NPG and AMPL depending upon composition), since there is limited solubility among the phases (i.e. no completely miscible solid solution as in PE–PG and high temperature PG–NPG).

Crystal structures for high temperature PE, NPG and AMPL are FCC, FCC and BCC respectively. Although PE and NPG are both FCC at high temperatures, they do not form a completely miscible solid solution, and there is a small two phase region $\gamma+\varepsilon$. This can be attributed to syncrystallization effect and the number of OH and $CH_3$ bonds in the compounds (this has been described in the PE–NPG binary phase diagram section). PE–AMPL binary system has two distinct high temperatures phases and the same pattern is also see in AMPL–NPG. Hence, it is assumed that there are three high temperature phases in the PE–NPG–AMPL system.

Fig. 8 shows six isotherms of PE–NPG–AMPL ternaries taken between 300 K and 450 K. Isopleths or pseudo-binary phase diagrams are plotted to determine continuous phase transitions in the PE–NPG–AMPL ternary system, at constant composition. Fig. 9 shows isopleths (0.2AMPL/0.4PE/0.4NPG) and a corresponding isotherm of PE–NPG–AMPL at 400 K. The isopleths AMPL composition is kept constant at 0.2 mole fraction. The blue dot in the ternary (Fig. 9) denotes composition that corresponds with the dot in the pseudo-binary (0.2AMPL/0.4PE/0.4NPG). At that specific composition and temperature, the isopleth as well as the isotherm shows a three phase region ($\alpha+\delta+\varepsilon$). Table B.2 in Appendix shows various transitions as a function of temperature using 0.2AMPL/0.4PE/0.4NPG isopleth. Keeping the composition fixed and increasing the temperature shows the continuous phase transitions taking place for that particular composition.

## 5. Conclusions

Thermodynamic calculations of pentaerythritol [PE-$C(CH_2OH)_4$], neopentylglycol [NPG-$(CH_3)_2C(CH_2OH)_2$] and 2-amino-2methyl-1,3, propanediol [AMPL-$(HOCH_2)_2C(NH_2)CH_3$] ternary phase diagram revealed a wider selection of solid solution materials available for practical thermal energy applications, as the experimental data of PE–NPG–AMPL ternary phase equilibria is not available in the literature. The PE–NPG–AMPL ternary system has been modeled by the CALPHAD method using available previous binary experimental data along with thermodynamic assessments of binary phase diagrams with the tie-lines and invariant equilibria composition and temperatures. Calculations of ternary PE–NPG–AMPL system were made from room temperature to the liquid phase by using substitutional solution model to optimize interaction parameters. The non-ideality of the solution phases were compensated by assuming various solution models; noting that an initial assumption of ideality of the high temperature phases was used only to estimate the metastable Gibbs energies of the binary systems. Calculated binary phase diagram of PE–NPG with isomorphous high temperature phases of PE and NPG facilitated the ternary calculations of PE–NPG–AMPL as there were incoherencies in the reported experimental data. The heat capacities did not play a significant role in calculations of PE–AMPL phase diagram as these solution phases are highly non-ideal, and this non-ideality has a dominating effect as compared to inclusion of heat capacities. Nevertheless, the heat capacities have been included in determining the Gibbs energies of the pure components. Pseudo-binary isopleths calculated from these ternary data will allow developing new solid solutions with a wide range of new composition and phase transition temperatures available for solid state thermal energy storage materials.

## Acknowledgments

The authors thank *Intel Corporation* for the financial support of this project. We are grateful to Murli Tirumala and Daryl Nelson for helpful discussions.

## Appendix A. Supporting information

Supplementary data associated with this article can be found in the online version at http://dx.doi.org/10.1016/j.calphad.2014.02.003.

## Appendix B. The auxiliary results

See Tables B.1 and B.2.

**Table B.1**
Experimental invariant equilibria for PE–AMPL system.

| Invariant equilibria | $X$ (mole fraction AMPL) | | | Temperature (K) |
|---|---|---|---|---|
| | $\alpha$ | $\delta$ | $\eta$ | |
| $\alpha+\eta\rightarrow\delta$ (peritectoid) | 0.35 | 0.9 | 0.95 | 357 |
| | $\alpha$ | $\gamma$ | $\eta$ | |
| $\gamma\rightarrow\alpha+\eta$ (eutectoid) | 0.2 | 0.6 | 0.65 | 423 |
| | $\gamma$ | $\eta$ | $L$ | |
| $\gamma+L\rightarrow\eta$ (peritectic) | 0.5 | 0.53 | 0.55 | 457 |

**Table B.2**
Various phase transitions as a function of temperature and varying concentration of PE and NPG, using 0.2AMPL/0.4PE/0.4NPG isopleth for the PE–NPG–AMPL ternary system.

| $X_{PE}$ | $X_{NPG}$ | Phase transitions |
|---|---|---|
| 0.7 | 0.1 | $\alpha+\beta+\delta \overset{297\ K}{\rightarrow} \alpha+\delta \overset{323\ K}{\rightarrow} \alpha+\varepsilon \overset{382\ K}{\rightarrow} L+\alpha+\varepsilon \overset{384\ K}{\rightarrow} L+\alpha \overset{421\ K}{\rightarrow} \alpha+\gamma \overset{450\ K}{\rightarrow} \gamma \overset{494\ K}{\rightarrow} L+\gamma \overset{505\ K}{\rightarrow} L$ |
| 0.6 | 0.2 | $\alpha+\beta+\delta \overset{237\ K}{\rightarrow} \alpha+\delta \overset{318\ K}{\rightarrow} \alpha+\varepsilon \overset{398\ K}{\rightarrow} L+\alpha+\varepsilon \overset{403\ K}{\rightarrow} L+\alpha \overset{422\ K}{\rightarrow} \alpha+\varepsilon+\gamma \overset{422.8\ K}{\rightarrow} \alpha+\gamma \overset{448\ K}{\rightarrow} \gamma \overset{479\ K}{\rightarrow} L+\gamma \overset{502\ K}{\rightarrow} L$ |
| 0.35 | 0.15 | $\alpha+\beta+\delta \overset{297\ K}{\rightarrow} \alpha+\delta+\varepsilon \overset{348\ K}{\rightarrow} \alpha+\gamma+\varepsilon \overset{353\ K}{\rightarrow} L+\alpha \overset{415\ K}{\rightarrow} L+\eta+\gamma \overset{423\ K}{\rightarrow} \gamma \overset{438\ K}{\rightarrow} L+\gamma \overset{477\ K}{\rightarrow} L$ |
| 0.1 | 0.4 | $\alpha+\beta+\delta \overset{297\ K}{\rightarrow} \alpha+\delta+\varepsilon \overset{338\ K}{\rightarrow} \alpha+\varepsilon \overset{3376\ K}{\rightarrow} L+\alpha+\varepsilon \overset{381\ K}{\rightarrow} L+\alpha \overset{420\ K}{\rightarrow} L+\gamma \overset{431\ K}{\rightarrow} L$ |
| 0.2 | 0.6 | $\alpha+\beta+\delta \overset{297\ K}{\rightarrow} \alpha+\beta+\varepsilon \overset{299\ K}{\rightarrow} \alpha+\varepsilon \overset{427\ K}{\rightarrow} \varepsilon \overset{432\ K}{\rightarrow} L+\varepsilon \overset{447\ K}{\rightarrow} L+\varepsilon+\gamma \overset{448\ K}{\rightarrow} L+\gamma \overset{452\ K}{\rightarrow} L$ |

## References

[1] D. Chandra, C.S. day, C.S. Barrett, Low- and high temperature structures of neopentylglycol plastic crystal, Powder Diffr. 8 (1993) 109.
[2] W.J. Dunning, Crystallographic studies of plastic crystals, J. Phys. Chem. Solids 18 (1961) 21.
[3] J. Timmermans, Plastic crystals: a historical review, J. Phys. Chem. Solids 18 (1961) 1.
[4] G.W. Gray, P.A. Winsor, Liquid Crystals and Plastic Crystals, Ellis Horwood Limited, Chichelster, Great Britain, 1974.
[5] L.A.K. Staveley, Thermodynamic studies of molecular rotation in solids, J. Phys. Chem. Solids 18 (1961) 46.
[6] D. Eilerman, R. Rudman, Refinement of pentaerythritol, Acta Crystallogr. B 35 (1979) 2458.
[7] R. Rudman, Solid State Commun. 29 (1979) 765.
[8] I. Nitta, T. Watanabe, X-ray investigation of the cubic modification of pentaerythritol, $C(CH_2OH)_4$, Bull. Chem. Soc. Jpn. 13 (1938) 28.
[9] D. Chandra, J.J. Fitzpatrick, C.S. Barrett, P.K. Fredecki, D.E. Levden (Eds.), Advances in X-ray Analysis, vol. 28, 1985, p. 353.
[10] E. Murrill, L. Breed, Solid–solid phase transitions determined by differential scanning calorimetry, Thermochim. Acta 1 (1970) 239.
[11] D.K. Benson, R.W. Burrows, J.D. Webb, Solid state phase transitions in pentaerythritol and related polyhydriv alcohols, Sol. Energy Mater. 13 (1986) 133.
[12] J. Font, J. Muntasell, J. Navarro, J.Ll. Tamarit, J. Lloveras, Calorimetric study of the mixtures PE/NPG and PG/NPG, Sol. Energy Mater. 15 (1987) 299.
[13] M. Barrio, J. Font, J. Muntasell, J. Navarro, J.Ll Tamarit, Applicability for heat storage of binary systems of neopentylglycol, pentaglycerine and pentaerythritol: a comparative analysis, Sol. Energy Mater. 18 (1988) 109.
[14] D. Chandra, C.S. Barrett, Final Report to the DOE Contract No. DE-AC03-84SF12205, 1986.
[15] D. Chandra, C.S. Barrett, D.K. Benson, Plenum Publishing, 1986, pp. 305–313.
[16] D. Chandra, C.S. Barrett, D.K. Benson, Plenum Publishing, 1986, pp. 609–616.
[17] M. Barrio, J. Font, D.O. Lopez, J. Muntasell, J.Ll. Tamarit, N.B. Chanh, Y. Haget, Binary-system neopentylglycol pentaglycerin, J. Chim. Phys. 87 (1990) 1835.
[18] D. Chandra, R.A. Lynch, W. Ding, J.J. Tomlinson, Advances in X-ray Analysis, vol. 33, 445.
[19] D. Chandra, Final Report to Oakridge National Laboratory Contract No. 19X-SC644V/DE-AC05-84 OR21400, 1990.
[20] J. Font, D.O. Lopez, J. Muntasell, J.Ll. Tamarit, Low temperature invariant in pentaerythritol/neopentylglycol binary system, Mater. Res. Bull. 24 (1989) 1251.
[21] M. Barrio, J. Font, D.O. Lopez, J. Muntasell, J.Ll. Tamarit, N.B. Chanh, Y. Haget, Determination of an intermediate cubic phase in the PE/NPG binary system by X-ray powder diffraction, J. Phys. Chem. Solids 52 (1991) 665.
[22] M. Teisseire, N.B. Chanh, M.A. Cuevas-Diarte, J. Guion, Y. Haget, D.O. Lopez, J. Muntasell, Calorimetry and X-ray diffraction investigations of the binary system neopentylglycol-pentaerythritol, Thermochim. Acta 181 (1991) 1.
[23] M. Barrio, J. Font, D.O. Lopez, J. Muntasell, J.Ll. Tamarit, N.B. Chanh, Y. Haget, M. Teisseire, J. Guion, X. Alcobe, Binary-system neopentylglycol pentaerythritol, J. Chim. Phys. 89 (1992) 695.
[24] J. Hansen, M.S. Thesis, University of Nevada, Reno, 1997.

[25] M. Barrio, D.O. Lopez, J.Ll. Tamarit, P. Negrier, Y. Haget, Degree of miscibility between non-isomorphous plastic phases: binary system NPG (neopentyl glycol)-TRIS [tris(hydroxymethyl)aminomethane], J. Mater. Chem. 5 (1995) 431.
[26] M. Barrio, J. Font, J. Muntasell, J.Ll. Tamarit, N.B. Chanh, Y. Haget, Binary-system neopentylglycol pentaglycerine, J. Chim. Phys. 87 (1990) 2455.
[27] M. Barrio, J. Font, D.O. Lopez, J. Muntasell, J.Ll. Tamarit, P. Negrier, N.B. Chanh, Y. Haget, Miscibility and molecular interactions in plastic phases: binary system pentaglycerin/ tris(hydroxymethyl)aminomethane, J. Phys. Chem. Solids 54 (1993) 171.
[28] M. Barrio, D.O. Lopez, J.Ll. Tamarit, P. Negrier, Y. Haget, Molecular interactions and packing in molecular alloys between nonisomorphous plastic phases, J. Solid State Chem. 124 (1996) 29.
[29] M. Barrio, J. Font, D.O. Lopez, J. Muntasell, J.Ll. Tamarit, Y. Haget, Plastic molecular alloys: the binary-system tris(hydroxymethyl)aminomethane 2-amino-2-methyl-1,3-propanediol, J. Chim. Phys. 91 (1994) 189.
[30] R. Russell, M.S. Thesis, University of Nevada, Reno, 1995.
[31] L. Sturz, V.T. Witusiewicz, U. Hecht, S. Rex, Organic alloy systems suitable for the investigation of regular binary and ternary eutectic growth, J. Cryst. Growth 270 (2004) 273.
[32] V.T. Witusiewicz,L. Sturz,U. Hecht, S. Rex, Thermodynamic description and unidirectional solidification of eutectic organic alloys: II. $(CH_3)_2C(CH_2OH)_2$–$(NH_2)(CH_3)C(CH_2OH)_2$ system, Acta Mater. 52 (2004) 5071 (Also see, V.T. Witusiewicz, L. Sturz, U. Hecht, S. Rex, Thermodynamic description and unidirectional solidification of eutectic organic alloys: IV. Binary systems neopentylglycol–succinonitrile and amino-methyl-propanediol–succinonitrile, Acta Mater. 53 (2005) 173.
[33] D.O. López, J. Salud, J. Ll. Tamarit, M. Barrio, H.A.J. Oonk, Uniform thermodynamic description of the orientationally disordered mixed crystals of a group of neopentane derivatives, Chem. Mater. 12 (2000) 1108.
[34] D. Chandra, W. Ding, R.A. Lynch, Phase transitions in “plastic crystals”, J. Less Common Met. 168 (1991) 159.
[35] M. Barrio, J. Font, D.O. Lopez, J. Muntasell, J.Ll. Tamarit, P. Negrier, Y. Haget, Miscibility in plastic phases: binary system NPG (neopentylglycol)/AMP (2-amino,2-methyl-1,3-propanediol), J. Phys. Chem. Solids 55 (1994) 1295.
[36] J. Salud, D.O. Lopez, M. Barrio, J.Ll. Tamarit, H.A.J. Oonk, P. Negrier, Y. Haget, On the crystallography and thermodynamics in orientationally disordered phases in two-component systems, J. Solid State Chem. 133 (1997) 536.
[37] R. Chellappa, D. Chandra, Phase diagram calculations of organic “plastic crystal” binaries: $(NH_2)(CH_3)C(CH_2OH)_2$–$(CH_3)_2C(CH_2OH)_2$ system, CALPHAD 27 (2003) 133.
[38] R. Chellappa, R. Russell, D. Chandra, Thermodynamic modeling of the $C(CH_2OH)_4$–$(NH_2)(CH_3)C(CH_2OH)_2$ binary system, CALPHAD 28 (2004) 3.
[39] A. Mishra, A. Talekar, D. Chandra, W-M Chien, Ternary phase diagram calculations of pentaerythritol–pentaglycerine–neopentylglycol system, vol. 535, 2012, pp. 17.
[40] J. Marrero, R. Gani, Group-contribution based estimation of pure component properties, Fluid Phase Equilibria 183 (2001) 183.
[41] D.O. Lopez, J. Van Braak, J.Ll. Tamarit, H.A.J. Oonk, Thermodynamic phase diagram analysis of three binary systems shared by five neopentane derivatives, CALPHAD 18 (1994) 387.
[42] D.O. Lopez, J. Van Braak, J.Ll. Tamarit, H.A.J. Oonk, Molecular mixed crystals of neopentane derivatives. A comparative analysis of three binary systems showing crossed isodimorphism, CALPHAD 19 (1995) 37.
[43] D. Eilerman, R. Lippman, R. Rudman, Polymorphism of crystalline poly (hydroxymethyl) compounds. VII. Structure and twinning of 2-(hydroxymethyl)-2-methyl-1,3-propanediol, Acta Crystallogr. B 39 (1983) 263.
[44] D Chandra, W-M Chien, V Gandikotta, D.W Lindle, Z. Phys. Chem. 216 (2002) 1433.
[45] M Barrio, J Font, D.O Lopez, J Muntasell, J.Ll Tamarit, Y Haget, Plasticmolecular alloys: the binary-system tris(hydroxymethyl)aminomethane 2-amino-2-methyl-1,3-propanediol, J. Chim. Phys. 91 (1994) 189.
[46] A.D Pelton, On the slopes of phase boundaries, Metall. Trans. A 19A (1988) 1819.
[47] M. Barrio, J. Font, J. Muntasell, J. Navarro, J.Ll. Tamarit, Applicability for heat-storage of binary-systems of neopentylglycol mixtures, Sol. Energy Mater. 18 (1998) 109.
[48] D. Chandra, Crystal Structure and Thermal Studies on Solid-State Energy Storage Materials, Final Report, Contract Number: 19X-SC644V/DE-AC05-84 OR21400, 1990.
[49] M. Teisseire, N.B. Chanh, M.A. Cuevas-Diarte, J. Guion, Y. Haget, D. Lopez, J. Muntasell, Thermochim. Acta 181 (1991) 1.
[50] D. Chandra, C.S. Barrett, Final Report to DOE, Contract No. DEAC03-84SF12205, January 1986.
[51] C.S. Chandra, Barrett, D.K Benson, Advances in X-ray Analysis, vol. 32, 609.
[52] N. Saunders, A.P Miodownik, Pergamon Materials Series,CALPHAD (Calculation of Phase Diagrams): A Comprehensive Guide, Elsevier Science Ltd, 1998.
[53] Thermo-Calc® User's Guide, Version N, Thermo-Calc Software AB, Stockholm, Sweden, 2000 (SD-008).
[54] A.D. Pelton, W.T. Thompson, Prog. Solid State Chem. 10 (1975) 119.